DLP 4D Printing of Multi-Responsive Bilayered Structures

*Philipp Mainik, Li-Yun Hsu, Claudius W. Zimmer, Dominik Fauser, Holger Steeb, and Eva Blasco**

Advances in soft robotics strongly rely on the development and manufacturing of new responsive soft materials. In particular, light-based 3D printing techniques, and especially, digital light processing (DLP), offer a versatile platform for the fast manufacturing of complex 3D/4D structures with a high spatial resolution. In this work, DLP all-printed bilayered structures exhibiting reversible and multi-responsive behavior are presented for the first time. For this purpose, liquid crystal elastomers (LCEs) are used as active layers and combined with a printable non-responsive elastomer acting as a passive layer. Furthermore, selective light response is incorporated by embedding various organic dyes absorbing light at different regimes in the active layers. An in-depth characterization of the single materials and printed bilayers demonstrates a reversible and selective response. Last, the versatility of the approach is shown by DLP printing a bilayered complex 3D structure consisting of four different materials (a passive and three different LCE active materials), which exhibit different actuation patterns when irradiated with different wavelengths of light.

1. Introduction

Active materials whose shape can be controlled on demand play a crucial role in the development of biomedical applications,[1]

P. Mainik, L.-Y. Hsu, C. W. Zimmer, E. Blasco
Institute for Molecular Systems Engineering and Advanced Materials
Heidelberg University
Im Neuenheimer Feld 225, 69120 Heidelberg, Germany
E-mail: eva.blasco@oci.uni-heidelberg.de
P. Mainik, L.-Y. Hsu, C. W. Zimmer, E. Blasco
Organic Chemistry Institute
Heidelberg University
Im Neuenheimer Feld 270, 29120 Heidelberg, Germany
D. Fauser, H. Steeb
Institute of Applied Mechanics
University of Stuttgart
Pfaffenwaldring 7, 70569 Stuttgart, Germany
H. Steeb
Stuttgart Center for Simulation Science
University of Stuttgart
Pfaffenwaldring 5a, 70569 Stuttgart, Germany

microfluidics,[2] as well as actuators and grippers in soft robotics.[3] Nature has been an extraordinary source of inspiration in this field. Notably, the design principles of many synthetic systems can be attributed to natural systems such as plants or animals, for example, flower blossom, Venus flytraps, gecko's feet, butterfly wings, or chameleon camouflage.[4,5] One of the simplest and most studied actuation systems using soft materials, both in simulation and experiments, are bilayers.[4] Bilayers usually consist of two distinct materials joined at an interface that are able to undergo bending. Often, an active and a passive layer is combined. In particular, the use of stimuli-responsive materials, such as responsive hydrogels[6] or liquid crystalline elastomers (LCEs)[7,8,9–11] as active layers, has been extensively explored within the last years. LCEs are excellent candidates due to their unique properties such as responsiveness to stimuli, tunable strength, elastic modulus, as well as multifunctionality.[12–14] Furthermore, using LCEs as active layers offers a fast response without the necessity of an aqueous environment.[12–14] Their response relies on a programmable anisotropy and its reversible switching between a liquid crystalline state and an isotropic state,[12–14] which also implies a volume and shape change in the direction of alignment of the liquid crystalline phase; and hence, a controlled shape transformation.[12–14] In particular, successful bending actuation has been demonstrated on LCEs bilayers using different stimuli.[7,11,15] For example, Schenning and coworkers reported dual-stimuli responsive bilayer actuators consisting of a light responsive LCE and a magnetic responsive polydimethylsiloxane (PDMS) containing iron particles.[11] Zhao and coworkers also showed bending behavior by NIR and UV-light irradiation on bilayers composed of LCE containing gold particles as active layer and polypropylene film as a passive layer.[7] However, the shape of these LCE-containing bilayers has been limited mainly to planar 2D sheet-like rectangular shapes prepared by molding techniques, and the study of complex 3D bilayer structures remained unexplored.

Recent progress on 3D/4D printing technologies has opened new possibilities enabling the fabrication of LCE structures with geometries that were simply unattainable in the past.[16,17] The fourth dimension refers to the possibility to change the shape or other properties of the 3D printed object over time upon stimulus. In particular, 3D printing techniques such as direct ink
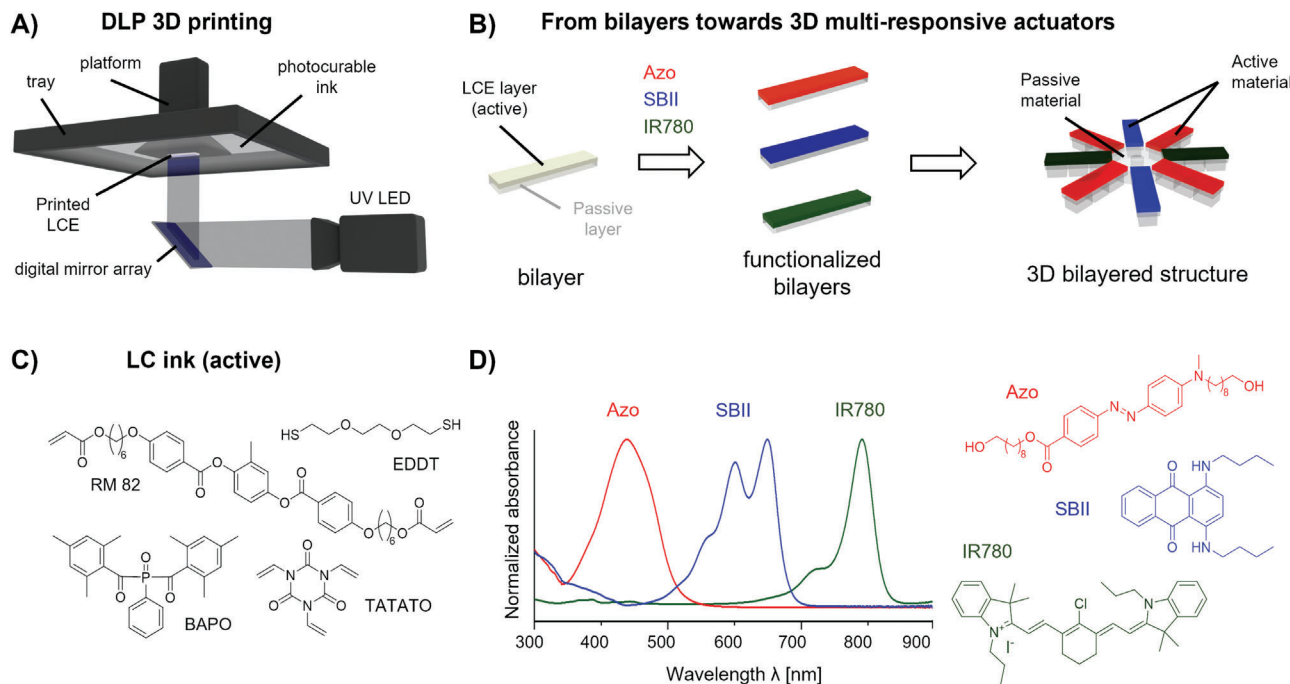
Figure 1. A) Schematic representation of the DLP 3D printing process. B) Models of the bilayers, consisting of LCEs and passive material, and multi-material 3D structures investigated in the present work. C) Composition of the LC formulation including the LC monomer RM82, EDDT, and TATATO, and BAPO as photoinitiator. D) Organic dyes incorporated in the LCE network and their absorption spectra in solution.

writing (DIW), extrusion-based methods, and light-based vat photopolymerization have been recently exploited for the manufacturing of LCE-based 4D structures.[16] On the one hand, DIW and extrusion-based methods have the advantages of enabling in situ LC alignment during the printing process by applied shearing forces.[18] Nevertheless, the resolution of the printed structures is limited to 100 µm by the nozzle diameter.[19,20] On the other hand, vat photopolymerization techniques allow for higher resolution and faster printing speed.[20] Within the last years, special attention has been paid to the development of new promising LCE inks for two-photon laser printing (2PLP)[21,22] and digital light processing (DLP),[9,10,23] enabling the manufacturing of complex micro- and macroscale 3D LC structures, respectively. Particularly, DLP 3D printing offers fast printing speed benefiting from its layer-by-layer fabrication while maintaining a high resolution of down to 30 µm (**Figure 1**A).[24] One of the drawbacks of the DLP technique is the lack of LC phase alignment during printing. For this reason, recent reports on DLP printing of LCEs have focused mainly on the development of in situ alignment procedures, for example, by platform shearing or switchable magnetic fields.[9,10] However, these examples concentrated on the DLP 3D printing of "single," temperature-responsive LCE materials, and to the best of our knowledge, there is no example of DLP 3D printed multi-material bilayered structures reported so far.

Herein, we introduce a versatile approach to all-printed multi-responsive actuators based on bilayered structures exhibiting reversible and complex actuation patterns using DLP printing. The structures consist of LCE as active layer and a printable non-responsive elastomer as passive layer (Figure 1B). Multi-response, and more specifically wavelength-selective light re-sponse, is achieved by embedding various organic dyes exhibiting absorption in different regions (from visible blue to near infrared [NIR] spectral range). The reversible actuation of bilayers upon heating or light exposure using different wavelengths is investigated in-depth. Furthermore, we demonstrate the potential of the presented approach by DLP printing a multi-material complex bilayered 3D structure which is able to execute three different bending patterns on-demand by irradiation at different wavelengths of light.

2. Results and Discussion

When seeking to fabricate complex and responsive geometries consisting of bilayered structures, the choice of the two compatible and DLP printable materials was crucial. To achieve this, as mentioned above, an LCE material was chosen as the active layer and a commercially available, elastic DLP printable material exhibiting a low Young's modulus (MPa regime) was used as the passive layer. The low Young's modulus of the passive layer ensured the compatibility of the passive layer with the LC material for successful bending. In the following paragraphs, the sequential steps starting from the rational design and characterization of the active material to the responsive bilayer, and last, to the fabrication of complex structure, are discussed.

2.1. Design and Printing of the Active Layer

Starting with the active material, we chose a main-chain LCE system consisting of a diacrylate-functionalized mesogen and dithiol

for chain extension. In a first step, the diacrylate-functionalized mesogen (RM82) and dithiol (EDDT) were oligomerized in the presence of triethylamine (2 wt%) and a multi-arm crosslinker (TATATO).[9] BHT (2 wt%) was added to this mixture to increase the thermal stability by acting as a radical scavenger. Subsequent photopolymerization in the DLP 3D printing process was achieved by addition of BAPO (2 wt%) acting as photoinitiator (Figure 1C). The addition of toluene as solvent was necessary to reduce the viscosity of the ink for subsequent DLP 3D printing. After oligomerization and stirring overnight, a Jacob's working curve was recorded using the LC formulation in a commercial DLP printer (Asiga Max X, $\lambda = 385$ nm, $I = 7.5$ mW cm^{-2}) to acquire the best printing parameters (Figure S1, Supporting Information). An exposure time of ≈ 5 s for a layer thickness of 100 μm was found to be optimal for printing.

In addition to the intrinsic temperature response of the LCE, we have further explored the possibility of incorporating selective light response by embedding various organic dyes absorbing at different regimes as photoabsorbers in a post-printing step. By doing so, a photothermal phase transition from the nematic to an isotropic state can be induced upon irradiation at suitable wavelengths where the dyes exhibit absorption. In particular, three different classes of dyes covering the whole visible to NIR spectral range, namely azobenzene, anthraquinone, and cyanine, were employed in this procedure. For this purpose, a push–pull azobenzene dye bearing nonyl alkyl chains for solubility was synthesized for its absorption maximum at 437 nm in the blue visible spectrum.[21] The anthraquinone dye Sudan Blue II (SBII) and the cyanine dye IR-780 iodide (IR780) are commercially available and show an absorption band around 620 and 780 nm, respectively (Figure 1D). The incorporation of these dyes was accomplished by immersing a DLP printed LCE in a dye solution (0.1 wt%) of chloroform for IR780 or toluene for Azo and SBII. In detail, this was facilitated by significant swelling of the LCE mesh in the solvents (swelling ratios $S_m = 2.6$ and $S_V = 3.4$ in toluene and $S_m = 9.8$ and $S_V = 6.8$ in chloroform), allowing thorough physical penetration of the dyes into the matrix. After removal of the solvent, the dyed samples recovered their initial dimensions. The successful entanglement of the dye in the LCE network was indicated by drastic color changes (Figure S2, Supporting Information). With this procedure, we avoided the challenges of using dyes in the final ink, such as solubility and photostability, as well as the compatibility with the LCE ink. The effect of the dye in the LC printed materials was studied by differential scanning calorimetry (DSC). The LCE (without dye) exhibited an endothermic nematic-to-isotropic transition temperature (T_{NI}) at ≈ 60 °C (Figure S3, Supporting Information). It was found that these post-printing processes did not alter the LC behavior of the material and only resulted in a slightly higher nematic-to-isotropic transition temperature (T_{NI}) of LCE at 67.3 °C for Azo, 67.7 °C for SBII, and 69.5 °C for IR780 (Figure S3, Supporting Information).

2.2. Characterization of the LCE Printed Layers

The next step was the in-depth characterization of the active printed LCE layers. For this purpose, 3D rectangular strips (10 mm × 3 mm × 1 mm) were printed using the optimized

formulation and printing parameters. To enable actuation in the desired direction, unidirectional stretching of the material with a force of 0.2 N leading to uniaxial alignment of the LCE network was applied (Figure S4, Supporting Information). The successful alignment was verified by polarized optical microscopy (Figure S5, Supporting Information). The alignment also affected the optical properties of the macroscopic material which turned from opaque to transparent. Upon removal of the uniaxial force, the strips remained in a stretched state with $L/L_0 = 1.4$ with L_0 and L being the lengths in the initial and deformed, that is, stretched configuration, respectively (**Figure 2**A,B; Figure S4, Supporting Information). The material behavior upon stretching was in agreement with previously reported polydomain LCEs in literature.[25]

First, the temperature response of the reference printed samples was investigated. In particular, two different experiments were conducted: In a first experiment, the stretched LCE printed samples were placed on a heating plate with the aim to study the shape recovery while heating to 70 °C (above T_{NI}) (Figure 2A). The elongated LCE fully contracted to the printed length upon heating to 70 °C within seconds. After allowing the strip to cool to room temperature, the process of programming and recovery could be repeated for at least six times without any noticeable change (Figure S6, Supporting Information). In a second experiment, the stretched LCE printed strips were kept at constant length and heated to 70 °C, while the change in the uniaxial mechanical properties had been monitored using a rheometer. Harmonic uniaxial excitations had been applied at a frequency of 1 Hz and with an amplitude in the linear viscoelastic regime. It was found that the stretched reference LCE possesses a storage modulus E' of 1.4 MPa at room temperature corresponding to the expected soft material properties for LCEs (Figure 2C).[14] Upon heating, the storage modulus E' decreased by around an order of magnitude (from 1.4 MPa to 230 kPa). Interestingly, the dyed LCEs showed slightly larger storage moduli E' of 2.8 to 5.3 MPa at room temperature (Figures S7–S9 and Table S1, Supporting Information). The decrease in E' in all the samples is related to the loss of liquid crystallinity upon phase transition from the aligned nematic to the isotropic state (Figure 2C; Figures S7–S9, Supporting Information).

Having characterized the temperature response, the light response of the dyed active printed layers was investigated. For this purpose, the printed specimens containing the different dyes were first stretched to the elongated states using the same procedure. After pre-conditioning, the samples were irradiated for 5 min and the complex Young's modulus E^* was measured with constant frequency and amplitude (Figure S10, Supporting Information). The normalized E^* (against maximum value) of the irradiated samples is depicted in Figure 2D. The irradiation wavelength for each dyed DLP printed LCE was selected according to the absorption bands of the dyes in solution being 459 nm for Azo, 622 nm for SBII, and 850 nm for IR780. It was observed that after irradiation the (absolute value of the) complex Young's moduli E^* of the dyed LCEs decreased instantaneously by more than an order of magnitude to an absolute value of 300 kPa, indicating the successful phase transition to the isotropic state (Figure S10, Supporting Information). Recording the irradiated dyed LCEs with a thermal camera revealed a rise of the surface temperature from 25 °C to more than 100 °C (Figures S11–S13,
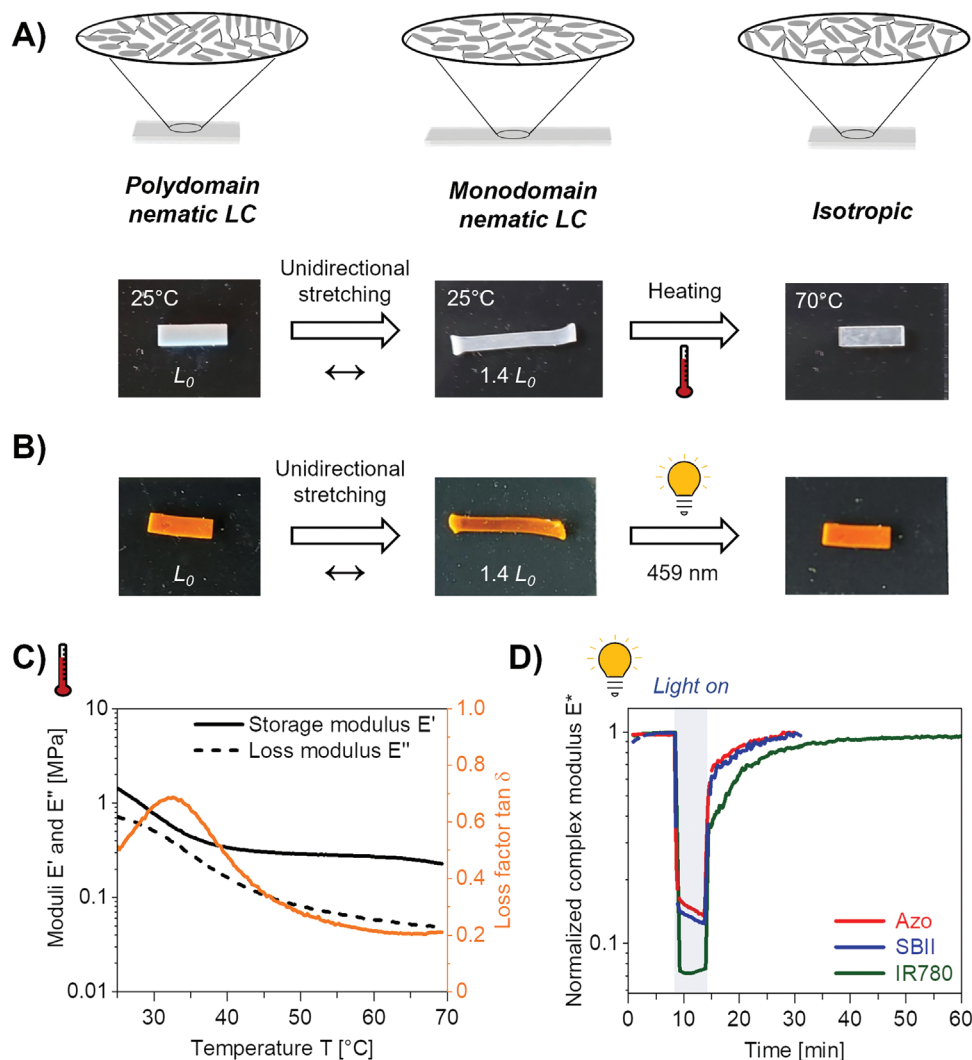
Figure 2. Characterization of the temperature and light response of the DLP printed LCE material. A) The reference blank LCE (10 mm × 3 mm × 1 mm) is stretched to induce alignment (the monodomain phase). Heating to 70 °C yields a phase transition to the isotropic state which results in the contraction of the active material. B) A DLP printed LCE (10 mm × 3 mm × 1 mm) doped with Azo is stretched. Upon irradiation at 459 nm, contraction of the active material is observed. Rheological measurements of the printed samples C) at different temperatures and D) upon light irradiation at the corresponding wavelengths.

Supporting Information). Switching off the light source led to an instantaneous first fast recovery which was followed by a slower recovery due to thermal conductivity of the LCEs yielding the initial Young's moduli. The behavior was similar for the different LCE samples with incorporated dyes. However, a slower recovery was observed for the LCE printed sample containing IR780 because the temperature reached in this experiment was higher (Figure S13, Supporting Information)

2.3. Bilayer Actuators

Once we optimized and characterized the active layers, we proceeded with combining the above studied LCE material with a non-responsive 3D printable elastomer which could act as a passive layer in bilayers. For the latter, we selected a commercially available DLP printable ink (FormFutura Engineering LCD Series Flex 82A Resin Clear). This material exhibits a low storage modulus of 3.3 MPa (Figure S14, Supporting Information), which is in the similar range as our printed LCEs; and therefore, compatible for the fabrication of the aimed bilayers. As before, the printing parameters of the passive ink were selected based on a recorded Jacob's working curve (Figure S15, Supporting Information) upon UV irradiation ($\lambda = 385$ nm, $I = 2.27$ mW cm^{-2}). With the optimized printing parameters for both materials, the final bilayers were prepared by adhering the stretched active layer to the passive layer (see details in the Experimental section).

Next, the response, that is, bending of the printed bilayer structures to external stimuli was studied. Similar as above, we first focused on the temperature response using the bilayer with the blank reference LCE active layers (**Figure 3**A). In a first experiment, the bilayered structures were placed in a water bath with
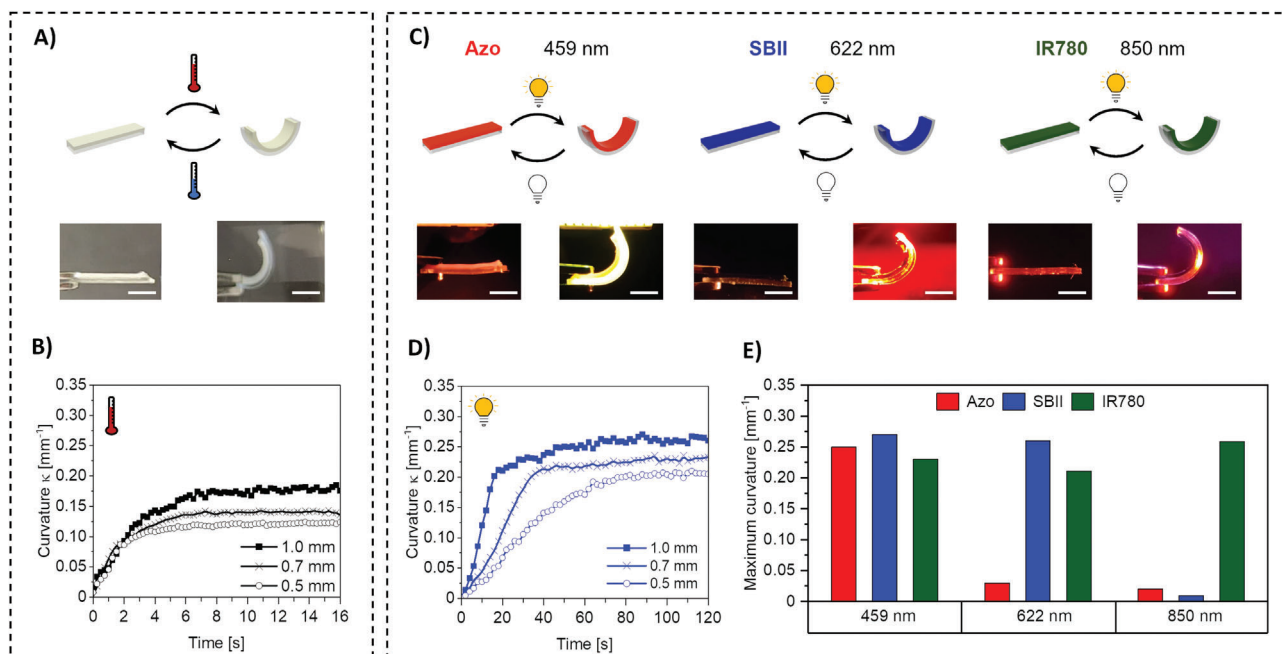
Figure 3. Characterization of the bending behavior of the bilayers with temperature and light irradiation. A) Schematic representation and photographs of the blank LCE bilayer upon heating. B) Bending of blank bilayers with varying LCE thickness in a water bath (70 °C). C) Schematic representation and photographs of the dyed bilayers upon irradiation at different wavelengths. D) Bending of SBII dyed bilayers with varying LCE thickness upon 622 nm light exposure. E) Wavelength-selective light-response of prepared multi-responsive bilayers with 1.00 mm LCE thickness containing the three different dyes. Scale bar: 5 mm.

varying temperatures from 40 °C to 80 °C. The largest change in curvature from 0.07 to 0.17 mm^{-1} was observed between 50 °C and 65 °C in the heating and cooling cycle (Figure S16, Supporting Information). This temperature range corresponds to the nematic-to-isotropic phase transition T_{NI} previously determined by DSC, meaning the maximum degree of actuation is reached after the phase transition. The bilayers with dyed LCEs showed higher curvatures upon heating compared to the blank LCE bilayers (Figure S16, Supporting Information). In addition to the temperature response upon slow heating (≈ 1 °C min^{-1}), we have analyzed the time response of the process by placing the bilayers directly inside a water bath which was pre-heated to 70 °C (Figure 3B). The analyzed bilayers (blank and with the three dyes) showed similar response times ranging from 6 to 8 s and maximum curvatures of 0.18–0.22 mm^{-1} (Figure 3B; Table S3, Supporting Information). The recovery times were 12–14 s and higher than the response times due to different heat conductivities of air and water in the experimental setup when introducing or removing the bilayer.

By varying LCE layer thickness in the bilayers from 0.5–1.0 mm, two effects in the response were observed. Reducing the LCE layer thickness, i.e., increasing the ratio of responsive to passive layer thickness, led to i) shorter response and recovery times with 4–7 s correlating with faster heating and cooling of the bilayers, and ii) a lower maximum in curvature upon stimulus (Figure 3B; Table S3, Supporting Information). These observations are in good agreement with a previously reported theoretical model derived by Timoshenko for bilayer bending structures.[26] Thus, the influence of the layer thickness on the response intensity can be used for careful design of the desired actuation system.

In a next step, the light response of the bilayers incorporating dyes in the LCE was analyzed (Figure 3C). The bilayers were irradiated with three selected LED wavelengths corresponding to the main absorption bands of the dyes in solution, respectively. In a first experiment, we irradiated the blank reference bilayers with the selected LEDs and did not observe any response, as expected (Table S4, Supporting Information). In contrast, reversible bending and unbending of the dyed bilayers were detected, proving the light response due to the incorporated dyes (Figure 3D; Table S4, Supporting Information). The response and recovery times for 90% of curvature change were reached within 30–60 s after switching on or off the light (Figure 3C; Table S4, Supporting Information). By altering the LCE thickness (0.5, 0.7, and 1.0 mm), the dyed bilayers followed the trend of the Timoshenko equation, similar to the previously analyzed temperature response (Figure S17, Supporting Information); though, increasing the LCE layer enhanced the bilayer response making the curvature tunable between 0.20 and 0.26 mm^{-1}. It is noteworthy that the detected curvature upon irradiation was higher than in the temperature response experiments. The larger curvature resulted from the larger temperature of the LCE in the experiment upon irradiation, as stated before. The higher temperature influences the mechanical properties of the LCE by reducing its Young's modulus. Remarkably, no significant changes in bending behavior were detected for all investigated bilayers in multiple actuation cycles (six cycles), proving the absence of considerable photobleaching, as well as a good longevity and reversibility of the process (Figures S18–S20, Supporting Information).

Importantly, in addition to the irradiation with corresponding wavelengths, we analyzed the wavelength-selectivity of the
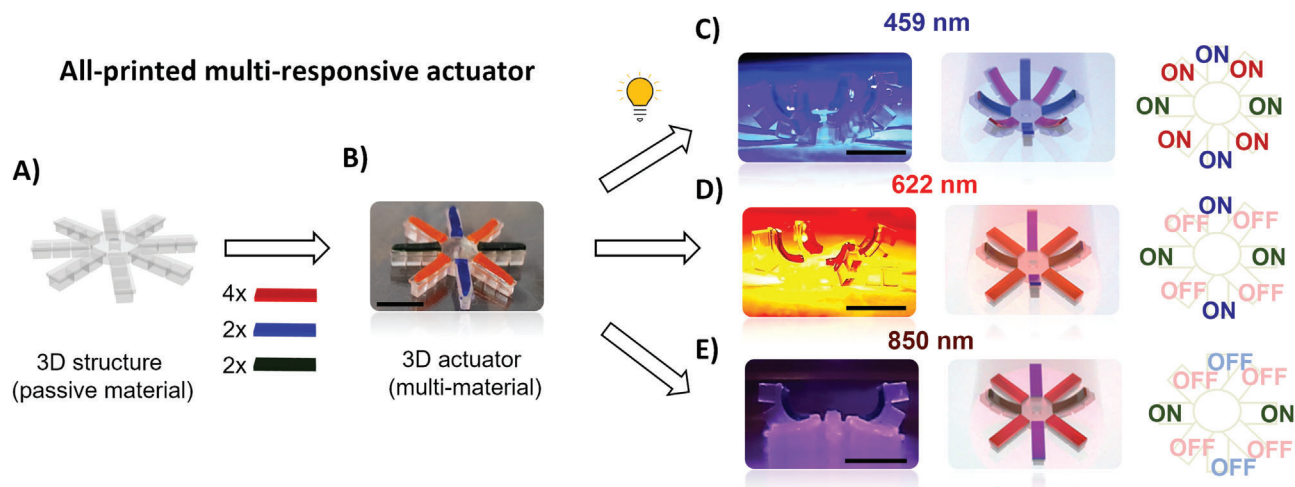
**ADVANCED
SCIENCE NEWS**
www.advancedsciencenews.com

**ADVANCED
MATERIALS
TECHNOLOGIES**
www.advmattechnol.de

Figure 4. Octopus-inspired DLP printed gripper-like multi-material structure. The gripper is prepared by combining A) a support structure with B) eight differently dyed printed LCE strips. The gripper shows a variety of distinct actuation patterns depending on the wavelength used for irradiation: C) Upon irradiation at 459 nm, the three differently dyed LCEs absorb; and therefore, all eight arms can be actuated. D) Upon irradiation with 622 nm light, the arms with SBII- and IR780 dyed LCEs bend selectively and E) at 850 nm, only the two opposite arms with IR780 dyed LCE layers bend. Scale bar: 1 cm.

bending motion. To this aim, each dyed LCE bilayer was irradiated with the three different light sources: a blue (459 nm), red (622 nm), and NIR (850 nm) LED. The Azo dyed LCE bilayers bent exclusively upon irradiation with the blue (459 nm) LED, and no actuation was observed using red (622 nm) and NIR (850 nm) LED irradiation. In the case of SBII dyed LCE bilayers, bending upon irradiation with the red LED was observed, as expected, because it lies in the absorption maxima of the dye. However, efficient actuation was also observed when irradiated with the blue LED despite the low absorption of the dye in this region. No bending was observed upon NIR LED irradiation. The IR780 dyed LCE bilayers showed bending upon irradiation with the three LEDs (blue, red, and NIR). The bending using blue and red light was also remarkable, despite the low absorption in the visible regime. Summarizing the wavelength selective observed (Figure 3D): using blue light (459 nm), the three bilayers can be actuated. By irradiation with red light (622 nm), SBII and IR780 dyed bilayers can be activated but not the Azo dyed bilayers. When irradiating with NIR light, only IR780 dyed bilayers yield a bending deformation. In addition, we also incorporated multiple dyes into DLP printed LCEs and showed the expected behavior (Table S5 and Figures S21–S26, Supporting Information).

2.4. Design and Printing of the Active Layer

The observed wavelength-selectivity was exploited for the fabrication of multi-material 3D structures to enable a new dimension of control over the actuation by using different irradiation wavelengths. Mimicking complex single moving octopus tentacles in nature, we designed a centimeter-sized gripper-like structure to prove the concept of wavelength-selective actuation patterns.

For this purpose, an eight-arm support structure was DLP 3D printed using the commercial passive elastomer (**Figure** 4A). In a second step, we 3D printed eight active LCE strips (8 mm × 3 mm × 1 mm) with dimensions fitting in their stretched state

to the arms of the support material (12 mm × 3 mm × 3 mm). The active layers were subsequently functionalized with Azo (4×), SBII (2×), and IR780 (2×), adhered onto the arms of the passive material support to yield a multi-material 3D structure (Figure 4B) and irradiated with three different wavelengths. By using the blue light irradiation source (459 nm), the bending of all arms was possible, showing the activation of all the dyed LCE materials, as proved before. When shifting to red light (622 nm), four out of eight arms were actuated because only the SBII and IR780 dyed arms were activated, while the four Azo dyed arms stayed inactive. Irradiating the gripper with the NIR LED emitting at 850 nm, the two opposite arms of the IR780 dyed LCE could be selectively activated and the Azo and SBII dyed arms remained flat. Thus, it was demonstrated that fine tuning the irradiation wavelength provides us with full control of achievable bending patterns.

3. Conclusion

We have presented a new approach for the fabrication of all-printed multi-responsive bilayered structures exhibiting reversible and complex actuation patterns using DLP as manufacturing technology. Versatile tailoring of the light responsiveness was easily performed by post-processing, avoiding tedious work with formulation and printer parameter optimization for all materials. This method was successfully employed for the preparation of LCEs with wavelength-selective behavior. Combining these printable multi-responsive LCE materials with passive materials into bilayers can be used as a modular approach enabling the design of a plethora of actuation patterns. In the near future, further efforts will be made in combining our presented system with reported in situ alignment methods suitable with DLP printing and by embedding other functionalities with our post-printing process. We believe that this work highlights the potential of 3D printing for the fabrication of new active structures

and paves the way toward the design of complex multi-material structures for soft robotics.

4. Experimental Section

Chemicals and Materials: 1,4-Bis[4-(3-acryloyloxyhexyloxy)benzoyloxy]-2-methylbenzene (RM82) was purchased from SYN-THON Chemicals GmbH & Co. KG. Formfutura Clear resin was purchased from 3Dmensionals/PONTIALIS. 1,3,5-Triallyl-1,3,5-triazine-2,4,6(1H,3H,5H)trione (TATATO), 2,2-(ethylenedioxy)diethanethiol (EDDT), 2,6-di-*tert*-butyl-4-methylphenol (BHT), phenylbis(2,4,6-trimethylbenzoyl)phosphine oxide (BAPO), IR-780 iodide (IR780), Sudan Blue II (SBII), and triethylamine (TEA) were purchased from Sigma–Aldrich. All solvents were supplied from either Sigma–Aldrich or Fisher Scientific unless otherwise mentioned. All commercial materials were used as received without further purification. The azobenzene dye Azo was synthesized and purified according to a previously reported method.[21] Light sensitive compounds such as acrylates and photoinitiators were stored in the dark and handled under yellow light.

LC Ink Preparation: RM82, EDDT, and TATATO were mixed in a molar ratio of 1.000:0.800:0.133 and dissolved in toluene (100 wt% - compared to RM82). After addition of BHT (2 wt%), BAPO (2 wt%), and triethylamine (2 wt%), the mixture was heated to 70 °C and stirred at this temperature for 2 h. Oligomerization was carried out in amber flasks. The flask was allowed to cool to room temperature at which time, the mixture was stirred for 18 h and used for DLP 3D printing.

Jacob's Working Curve: Prior to DLP printing, Jacob's working curves were recorded for LCE and Formfutura Clear by irradiating resin drops on a 0.16 mm thin glass slide with a UV-emitting LED (385 nm) in the DLP printer with different irradiation times at fixed intensity. The irradiated circular spot size was set to 5.00 mm in diameter. The intensity of the LED was adjusted to calibrate a cure depth of 0.10 mm for subsequent DLP printing in a time range between 3 and 8 s. Unpolymerized resin was removed with isopropanol and acetone for both materials. After drying the material carefully under nitrogen flow, the thicknesses of the polymer films were determined using a digital caliper (precision: 0.01 mm).

DLP Printing: DLP printing was performed with a commercial Asiga MAX X with an integrated UV-emitting LED at 385 nm with a pixel resolution of 27 µm. 3D models were created with the open-source model software Blender 2.90 and exported as stl files. These files were uploaded to the Asiga Composer Software together with the customized initiation files based on the experimentally determined Jacob's working curve. A customized platform and vat were used to reduce ink usage and enable 3D printing with 4 to 5 mL of resin for printing of the LCE. Models were printed with a slice thickness of 0.10 mm at 25 °C. Unpolymerized resin was removed by rinsing with isopropanol and acetone for all printed structures. After development, all materials were dried in a vacuum oven at 25 °C for 18 h and stored protected from light. Polymer samples were dried in a Thermo Scientific Vacutherm vacuum oven. Irradiation intensity was measured with a PM100D power meter from Thorlabs.

Dye Immersion: For dye incorporation, Azo and SBII were dissolved in toluene solutions, and IR780 in a chloroform solution. Dye immersion in the LCEs was performed by placing LCE strips in these solutions with dye concentrations of 0.1 wt%. After 24 h, the solvent was removed, and the strips were dried in a vacuum oven for 1 h. The dyed strips were washed and kept with isopropanol (4 × 1 h) and dried in the vacuum oven for 18 h. Note: the blank samples were treated with the same procedure using pure organic solvents.

Preparation of Bilayers: Passive layers with dimensions of 15 mm × 3 mm × 0.7 mm and active (dyed) layers with 10 mm × 3 mm with different thickness were printed using DLP in order to study the influence of the active layer thickness on the bending behavior. The length of the printed passive layer corresponded to the length of the elongated active (dyed) layers in the programmed state, that is, stretched state with $L/L_0 = 1.4$. In detail, LCE strip ends of the longer axis were fixed with paper clips between two glass slides. The strips were stretched by attaching a glass vial filled with 20 g of sand on the lower paper clip. The stretching of the strips was performed for 1 min until the weight, paper fold clips, and glass sides were removed. The stretched LCE strips were adhered to Formfutura Clear strips with a UV-curable glue (Norland UV Sealant 91). The bilayer was photocured for 30 min in an Asiga Flash UV chamber.

Analysis of Stimuli Response: Analysis of the stimuli responses was carried out using videos recorded with a Xiaomi Redmi Note 9 Pro. Snapshots of the recorded videos were extracted using the software FFmpeg 4.4.1 and further calibrated and analyzed with ImageJ 1.53j. Curvature was determined by selecting three points at the interface between passive and LCE layer to generate a circle. The curvature κ was determined with image analysis by fitting a circle to the three points (Figure S27, Supporting Information). Temperature response was measured with a water bath. Light response experiments were performed using an Osram OSTAR High Power Projection LED with emitting wavelengths of 459 and 622 nm, as well as an OSRAM IR OSLON Black 16 Cluster for IR light with an emitting wavelength of 850 nm. Intensities used for irradiation were 0.16 W cm^{-2} (459 nm), 0.25 W cm^{-2} (622 nm), and 0.67 W cm^{-2} (850 nm). Response and recovery times were determined as 90% of the total curvature change. Data processing was performed with Origin 2022.

Preparation of Multi-Material Gripper: A passive gripper-like support with eight 10 mm × 3 mm × 10 mm arms was printed with the Formfutura Clear resin. Eight LCE strips with dimensions of 6 mm × 3 mm × 1 mm were printed. Two of these films were immersed in a SBII or IR780 dye solution (0.1 wt%), respectively. Four of the remaining eight LCE strips were immersed in an Azo dye solution (0.1 wt%) in toluene. After drying all eight strips and washing them with isopropanol (four times), they were elongated to $L/L_0 = 1.4$ following the stretching procedure. The elongated strips were glued with a UV-curable glue to the arms of the passive printed gripper-like support. The multi-material structure was photocured for 3 min in an Asiga Flash UV chamber.

Supporting Information

Supporting Information is available from the Wiley Online Library or from the author.

Conflict Of Interest

The authors declare no conflict of interest.

Data Availability Statement

The data that support the findings of this study are available from the corresponding author upon reasonable request.

[1] a) E. Cabane, X. Zhang, K. Langowska, C. G. Palivan, W. Meier, *Biointerphases* **2012**, *7*, 9; b) D. Schmaljohann, *Adv. Drug Delivery Rev.* **2006**, *58*, 1655; c) C. de Las Heras Alarcon, S. Pennadam, C. Alexander, *Chem. Soc. Rev.* **2005**, *34*, 276.

[2] a) W. Hilber, *Appl. Phys. A* **2016**, *122*, 751; b) A. Sánchez-Ferrer, T. Fischl, M. Stubenrauch, A. Albrecht, H. Wurmus, M. Hoffmann, H. Finkelmann, *Adv. Mater.* **2011**, *23*, 4526.

[3] a) J. Shintake, V. Cacucciolo, D. Floreano, H. Shea, *Adv. Mater.* **2018**, *30*, 1707035; b) C. Majidi, *Adv. Mater. Technol.* **2018**, *4*, 1800477; c) N. El-Atab, R. B. Mishra, F. Al-Modaf, L. Joharji, A. A. Alsharif, H. Alamoudi, M. Diaz, N. Qaiser, M. M. Hussain, *Adv. Intell. Syst.* **2020**, *2*, 2000128; d) E. Sachyani Keneth, A. Kamyshny, M. Totaro, L. Beccai, S. Magdassi, *Adv. Mater.* **2021**, *33*, 2003387. e) F. Ilievski, A. D. Mazzeo, R. F. Shepherd, X. Chen, G. M. Whitesides, *Angew. Chem.* **2011**, *123*, 1930.

[4] a) R. Kempaiah, Z. Nie, *J. Mater. Chem. B* **2014**, *2*, 2357; b) X. Sun, L. Yue, L. Yu, H. Shao, X. Peng, K. Zhou, F. Demoly, R. Zhao, H. J. Qi, *Adv. Funct. Mater.* **2022**, *32*, 2109805.

[5] W. Li, Q. Guan, M. Li, E. Saiz, X. Hou, *Prog. Polym. Sci.* **2023**, *140*, 101665.

[6] a) V. Chan, K. Park, M. B. Collens, H. Kong, T. A. Saif, R. Bashir, *Sci. Rep.* **2012**, *2*, 857; b) X. Liu, J. Liu, S. Lin, X. Zhao, *Mater. Today* **2020**, *36*, 102; c) Z. Hu, X. Zhang, Y. Li, *Science* **1995**, *269*, 525; d) S.-J. Jeon, A. W. Hauser, R. C. Hayward, *Acc. Chem. Res.* **2017**, *50*, 161; e) L. Ionov, *Mater. Today* **2014**, *17*, 494.

[7] X. Lu, H. Zhang, G. Fei, B. Yu, X. Tong, H. Xia, Y. Zhao, *Adv. Mater.* **2018**, *30*, 1706597.

[8] a) C. L. van Oosten, C. W. M. Bastiaansen, D. J. Broer, *Nat. Mater.* **2009**, *8*, 677; b) F. Greco, V. Domenici, A. Desii, E. Sinibaldi, B. Zupančič, B. Zalar, B. Mazzolai, V. Mattoli, *Soft Matter* **2013**, *9*, 11405; c) L. T. de Haan, J. M. N. Verjans, D. J. Broer, C. W. M. Bastiaansen, A. P. H. J. Schenning, *J. Am. Chem. Soc.* **2014**, *136*, 10585; d) X. Lu, S. Guo, X. Tong, H. Xia, Y. Zhao, *Adv. Mater.* **2017**, *29*, 1606467; e) J. M. Boothby, T. H. Ware, *Soft Matter* **2017**, *13*, 4349; f) A. Agrawal, T. Yun, S. L. Pesek, W. G. Chapman, R. Verduzco, *Soft Matter* **2014**, *10*, 1411; g) *Smart Materials in Additive Manufacturing* (Eds: M. Bodaghi, A. Zolfagharian), Elsevier, Amsterdam, the Netherlands **2022**.

[9] S. Li, H. Bai, Z. Liu, X. Zhang, C. Huang, L. W. Wiesner, M. Silberstein, R. F. Shepherd, *Sci. Adv.* **2021**, *7*, eabg3677.

[10] M. Tabrizi, T. H. Ware, M. R. Shankar, *ACS Appl. Mater. Interfaces* **2019**, *11*, 28236.

[11] M. Da Pilz Cunha, Y. Foelen, T. A. P. Engels, K. Papamichou, M. Hagenbeek, M. G. Debije, A. P. H. J. Schenning, *Adv. Opt. Mater.* **2019**, *7*, 1801604.

[12] C. Liu, H. Qin, P. T. Mather, *J. Mater. Chem.* **2007**, *17*, 1543.

[13] C. Ohm, M. Brehmer, R. Zentel, *Adv. Mater.* **2010**, *22*, 3366.

[14] K. M. Herbert, H. E. Fowler, J. M. McCracken, K. R. Schlafmann, J. A. Koch, T. J. White, *Nat. Rev. Mater.* **2022**, *7*, 23.

[15] a) M. Gastaldi, F. Cardano, M. Zanetti, G. Viscardi, C. Barolo, S. Bordiga, S. Magdassi, A. Fin, I. Roppolo, *ACS Mater. Lett.* **2021**, *3*, 1; b) D. E. Hagaman, S. Leist, J. Zhou, H. F. Ji, *ACS Appl. Mater. Interfaces* **2018**, *10*, 27308; c) B. Zuo, M. Wang, B.-P. Lin, H. Yang, *Nat. Commun.* **2019**, *10*, 4539.

[16] Z. Guan, L. Wang, J. Bae, *Mater. Horiz.* **2022**, *9*, 1825.

[17] a) M. O. Saed, A. Gablier, E. M. Terentjev, *Chem. Rev.* **2022**, *122*, 4927; b) C. A. Spiegel, M. Hippler, A. Münchinger, M. Bastmeyer, C. Barner-Kowollik, M. Wegener, E. Blasco, *Adv. Funct. Mater.* **2020**, *30*, 1907615.

[18] a) Y. Wang, R. Yin, L. Jin, M. Liu, Y. Gao, J. Raney, S. Yang, *Adv. Funct. Mater.* **2023**, *33*, 2210614; b) C. Zhang, X. Lu, G. Fei, Z. Wang, H. Xia, Y. Zhao, *ACS Appl. Mater. Interfaces* **2019**, *11*, 44774; c) D. J. Roach, X. Sun, X. Peng, F. Demoly, K. Zhou, H. J. Qi, *Adv. Funct. Mater.* **2022**, *32*, 2203236; d) X. Peng, S. Wu, X. Sun, L. Yue, S. M. Montgomery, F. Demoly, K. Zhou, R. R. Zhao, H. J. Qi, *Adv. Mater.* **2022**, *34*, 2204890; e) M. O. Saed, C. P. Ambulo, H. Kim, R. De, V. Raval, K. Searles, D. A. Siddiqui, J. M. O. Cue, M. C. Stefan, M. R. Shankar, T. H. Ware, *Adv. Funct. Mater.* **2019**, *29*, 1806412; f) A. Kotikian, R. L. Truby, J. W. Boley, T. J. White, J. A. Lewis, *Adv. Mater.* **2018**, *30*, 1706383; g) W. Liao, Z. Yang, *Mater. Horiz.* **2023**, *10*, 576; h) J. Sgotti Veiga, M. Reis Carneiro, R. Molter, M. Vinciguerra, L. Yao, C. Majidi, M. Tavakoli, *Adv. Mater. Technol.* **2023**, 2300144.

[19] M. A. S. R. Saadi, A. Maguire, N. T. Pottackal, M. S. H. Thakur, M. M. Ikram, A. J. Hart, P. M. Ajayan, M. M. Rahman, *Adv. Mater.* **2022**, *34*, 2108855.

[20] S. C. Ligon, R. Liska, J. Stampfl, M. Gurr, R. Mülhaupt, *Chem. Rev.* **2017**, *117*, 10212.

[21] L.-Y. Hsu, P. Mainik, A. Münchinger, S. Lindenthal, T. Spratte, A. Welle, J. Zaumseil, C. Selhuber-Unkel, M. Wegener, E. Blasco, *Adv. Mater. Technol.* **2023**, *8*, 2200801.

[22] a) A. Münchinger, L.-Y. Hsu, F. Fürniß, E. Blasco, M. Wegener, *Mater. Today* **2022**, *59*, 9; b) H. Zeng, P. Wasylczyk, C. Parmeggiani, D. Martella, M. Burresi, D. S. Wiersma, *Adv. Mater.* **2015**, *27*, 3883; c) F. Zhang, L. Zhu, Z. Li, S. Wang, J. Shi, W. Tang, N. Li, J. Yang, *Addit. Manuf.* **2021**, *48*, 102423; d) M. Del Pozo, C. Delaney, C. W. M. Bastiaansen, D. Diamond, A. P. H. J. Schenning, L. Florea, *ACS Nano* **2020**, *14*, 9832.

[23] a) N. A. Traugutt, D. Mistry, C. Luo, K. Yu, Q. Ge, C. M. Yakacki, *Adv. Mater.* **2020**, *32*, 2000797; b) C. Luo, C. Chung, N. A. Traugutt, C. M. Yakacki, K. N. Long, K. Yu, *ACS Appl. Mater. Interfaces* **2021**, *13*, 12698.

[24] R. Liska, M. Schuster, R. Inführ, C. Turecek, C. Fritscher, B. Seidl, V. Schmidt, L. Kuna, A. Haase, F. Varga, H. Lichtenegger, J. Stampfl, *J. Coat. Technol. Res.* **2007**, *4*, 505.

[25] N. A. Traugutt, R. H. Volpe, M. S. Bollinger, M. O. Saed, A. H. Torbati, K. Yu, N. Dadivanyan, C. M. Yakacki, *Soft Matter* **2017**, *13*, 7013.

[26] a) Y. Cui, C. Wang, K. Sim, J. Chen, Y. Li, Y. Xing, C. Yu, J. Song, *AIP Adv.* **2018**, *8*, 025215; b) S. Timoshenko, *J. Opt. Soc. Am.* **1925**, *11*, 233; c) T. van Manen, S. Janbaz, A. A. Zadpoor, *Mater. Today* **2018**, *21*, 144.